Synthesis, Structures and Physical Properties of Bis(ethylenedithio)tetrathiafulvalenium Salts of Paramagnetic Metallacarborane Anions†

Yaw-Kai Yan,[a] D. Michael P. Mingos,*[,a] David J. Williams[a] and Mohamedally Kurmoo[b]

[a] *Department of Chemistry, Imperial College of Science, Technology and Medicine, South Kensington, London SW7 2AY, UK*

[b] *The Royal Institution of Great Britain, 21 Albemarle Street, London W1X 4BS, UK*

Single phases of the bis(ethylenedithio)tetrathiafulvalenium (et^{+}) salts $[et]_2[Cr(1,2\text{-}C_2B_9H_{11})_2]$ **1** and $[et]_2[Fe\{1\text{-}SC_4H_3\text{-}1,2\text{-}C_2B_9H_{10}\}_2]$ **2** (SC_4H_3 = thiophen-2-yl) were synthesised *via* chemical and electrochemical routes, respectively. The crystal structures of both salts feature alternating layers of et units and metallacarborane anions. The packing motif of **1** is very similar to that of the β′-$[et]_2X$ salts {X = $[ICl_2]^-$ or $[BrICl]^-$}, with the rod-shaped $[Cr(C_2B_9H_{11})_2]^-$ anions functioning as paramagnetic analogues of the trihalide anions and the et units being linked by short intermolecular S···S interactions (3.4–3.6 Å) to form one-dimensional 'tapes' extending in the (1 0 0) direction. The et units in **2** are packed more evenly, resulting in a two-dimensional honeycomb network of short intermolecular S···S interactions (3.4–3.6 Å) within each et layer. The $[Fe(C_2B_9H_{10}C_4H_3S)_2]^-$ anions in **2** pack to form unusual double-layers in which the thiophene groups are oriented towards each other and away from the et layers, indicating that inter-et S···S interactions are favoured over et–thiophene S···S interactions. Both compounds **1** and **2** are semiconductors with complex temperature-dependent conductivities between *ca.* 75 and 280 K. Their conductivities at room temperature are *ca.* 2×10^{-3} S cm^{-1} (**1**, compressed pellet) and 5×10^{-1} S cm^{-1} (**2**, single crystals). The absence of metallic behaviour in **1** and **2** may be attributed in part to the loose packing of the et molecules, due to the large size of the anions, in these compounds. The magnetic susceptibilities of **1** and **2** were fitted by the Curie–Weiss law between 25 and 300 K to give Weiss constants of −1.1 and +1.6 K respectively.

Amongst the electron-donor molecules employed as components of organic conductors, bis(ethylenedithio)tetrathiafulvalene (et) has yielded the largest number of superconducting cation-radical salts.[1] The crystal structures of the et salts usually consist of alternating layers of et and anion molecules. The conducting behaviour of these salts are determined by their electronic and vibronic properties, which to a large extent are determined by the molecular packing and donor–donor and donor–anion interactions.[1,2] Thus, the size and shape of the anions and the thickness of the anion layers are important factors governing the electrical properties of cation-radical salts of et. In the β-$[et]_2X$ series of salts (X = linear triatomic monoanion), for example, whilst the isostructural $[I_3]^-$, $[AuI_2]^-$ and $[IBr_2]^-$ salts[3–5] (type II in the nomenclature of Williams *et al.*)[1] are superconductors with transition temperatures (T_cs) of 8, 5.0 and 2.8 K respectively, the salts of the smaller $[ICl_2]^-$ and $[BrICl]^-$ anions (type I or β′-phases) are semiconductors.[6] This difference in behaviour has been attributed to the more anisotropic packing of et molecules in the type I salts, which results in one-dimensional electronic band structures.[7] For the type II salts, the T_cs increase with increasing anion size {$[IBr_2]^-$ < $[AuI_2]^-$ < $[I_3]^-$}, although the T_c of 8 K for β-$[et]_2I_3$ is attained with slight pressure (≈0.5 kbar) and shear.[3]

As part of our study of cation-radical salts of metallacarborane anions,[8] the et salts of the complexes *commo*-[3,3′-Cr(1,2-$C_2B_9H_{11})_2]^-$ and *commo*-$[3,3'\text{-}Fe\{1\text{-}SC_4H_3\text{-}1,2\text{-}C_2B_9H_{10}\}_2]^-$ (SC_4H_3 = thiophen-2-yl) were synthesised. The use of monoanionic bis(dicarbollyl)metal complexes in this area is of interest because the complexes are rod-shaped and many of them are paramagnetic, making them good candidates for components of magnetic analogues of the existing β-phase et salts. The study of such materials may contribute to the understanding of the relationship between magnetism and superconductivity.[9] In particular, the chromacarborane complex chosen for study here combines high prolateness (length 12.8 Å, maximum cross-sectional radius 3.7 Å) and high spin ($S = \frac{3}{2}$). Although its prolateness is close to that of the $[ICl_2]^-$ anion (length 8.7 Å, maximum cross-sectional radius 2.2 Å),[1a] its length exceeds that of the $[I_3]^-$ anion (10.1 Å).[1a] It is of interest to find out which of these parameters have a greater effect on the arrangement of et molecules in the cation-radical salt. The thiophene-substituted ferracarborane $[Fe\{1\text{-}SC_4H_3\text{-}1,2\text{-}C_2B_9H_{10}\}_2]^-$ (SC_4H_3 = thiophen-2-yl) ($S = \frac{1}{2}$) is overall more discoidal in shape and hence is expected to favour a different packing motif of the et molecules. Since weak ferromagnetic interactions have been observed in the tetrathiafulvalenium (ttf) salts of this anion (θ = 1.9 and 0.5 K for $[ttf]_5[Fe(C_2B_9H_{10}C_4H_3S)_2]_2$ and $[ttf][Fe(C_2B_9H_{10}C_4H_3S)_2]$ respectively),[8b] it was hoped that the anion would favour ferromagnetic interactions in its et salt as well.

It is also noteworthy that the majority of the reported et salts were prepared by electrocrystallisation. Chemical oxidation has

† Bis(ethylenedithio)tetrafulvalene is more systematically named 4,5-ethylene(dithio)-2-[4,5-(ethylenedithio)dithiol-2-ylidene]-1,3-dithiole.

Supplementary data available: see Instructions for Authors, *J. Chem. Soc., Dalton Trans.*, 1995, Issue 1, pp. xxv–xxx.

Non-SI units employed: bar = 1×10^5 Pa, eV ≈ 1.60×10^{-19} J, $\mu_B \approx 9.274 \times 10^{-24}$ J T^{-1}.

only been employed in a few cases in which oxidising precursors such as polyhalides and copper(II) halides were used.[1b,10] In most other cases, the lack of oxidising precursors for the anions precluded synthesis by direct charge-transfer reactions. Although electrocrystallisation is the best method for obtaining large single crystals of high quality, the conventional electrocrystallisation apparatus suffers from the limitation that only a small amount of material can be produced each time. Furthermore, multiple phases are often formed at a single electrode and the relative yields of each phase are sensitive to subtle differences in crystallisation conditions.[1] A reliable general method for the synthesis of et salts *via* chemical oxidation is thus desirable. With the aim of developing such a method, the synthesis of $[et]_2[Cr(C_2B_9H_{11})_2]$ by chemical oxidation was attempted.

The syntheses of the salts $[et]_2[Cr(C_2B_9H_{11})_2]$ **1** and $[et]_2[Fe(C_2B_9H_{10}C_4H_3S)_2]$ **2** are reported in this paper, together with their crystal structures, magnetic properties and electrical conductivities.

Results and Discussion

(*a*) *Syntheses.*—(*i*) $[et]_2[Cr(C_2B_9H_{11})_2]$ **1**. On addition of H_2O_2 to a tetrahydrofuran (thf) solution of et and $H[Cr(C_2B_9H_{11})_2]$ at room temperature, the solution turned dark red-violet and shiny bronze needles of compound **1** slowly precipitated [equation (1)].

$$4\,et + 2\,H[Cr(C_2B_9H_{11})_2] + H_2O_2 \longrightarrow 2[et]_2[Cr(C_2B_9H_{11})_2] + 2\,H_2O \quad (1)$$

A low yield (25%) of the product was obtained, and cooling the mother-liquor to −20 °C resulted only in the crystallisation of unreacted et.

The use of *p*-benzoquinone and 2,3-dichloro-5,6-dicyano-*p*-benzoquinone (ddq) as oxidising agents resulted in better yields of compound **1** (42 and 52% respectively).

In all preparations, the crystals of **1** obtained were homogeneous both in morphology and colour. There was no evidence that a second phase was formed.

When the reaction with *p*-benzoquinone was carried out with 1,1,2-trichloroethane as the solvent, a dark brown solution was obtained. Storage of the solution at −20 °C overnight afforded only a trace amount of brown powdery precipitate.

Attempts were also made to grow larger crystals of compound **1** by slow inter-diffusion of thf solutions of et–$H[Cr(C_2B_9H_{11})_2]$ and H_2O_2 or *p*-benzoquinone through a glass frit at room temperature under nitrogen. No crystals were formed in either case. This may be because the rate of decomposition of compound **1** in thf solution is greater than that of crystal nucleation. It was observed in separate experiments that brown solutions of compound **1** in thf slowly turn light orange (20 h) at room temperature under nitrogen. The process occurs within 5 min in boiling thf.

(*ii*) $[et]_2[Fe(C_2B_9H_{10}C_4H_3S)_2]$ **2**. Compound **2** was prepared by constant-current anodic oxidation of et in the presence of $[NBu^n_4][Fe(C_2B_9H_{10}C_4H_3S)_2]$ in 1,1,2-trichloroethane. The electrocrystallisation was carried out under nitrogen in a two-chamber H-cell in which the anodic and cathodic compartments were separated by a fine-porosity glass frit. Black plate-like crystals of **2** were formed at the bottom of the anodic chamber after 2 to 4 weeks. Although no other crystalline phases were detected, the crystals of **2** obtained were contaminated by a small amount of a powdery, straw-coloured material which was insoluble in acetone or 1,1,2-trichloroethane. This impurity could be removed by repeatedly suspending the mixture in acetone and decanting off the impurity-containing suspension once the crystals of **2** had settled.

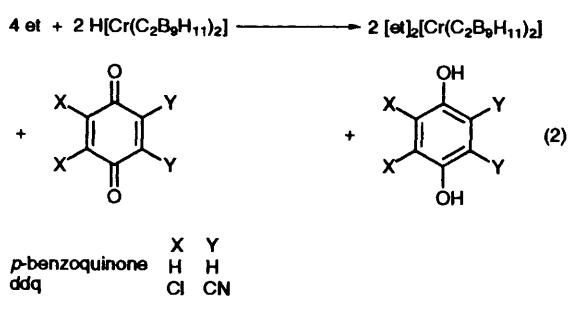

(*b*) *Crystal Structures.*—(*i*) $[et]_2[Cr(C_2B_9H_{11})_2]$ **1**. Compound **1** crystallises in the triclinic space group $P\bar{1}$. The asymmetric unit contains one et molecule and half a bis(dicarbollyl)chromium unit. The remainder of the $[Cr(C_2B_9H_{11})_2]^-$ anion is generated by inversion about the Cr centre at $(0, -\frac{1}{2}, \frac{1}{2})$. The atomic numbering schemes for the et molecule and $[Cr(C_2B_9H_{11})_2]^-$ anion are shown in Fig. 1.

The bond lengths within the et molecules (see Table 1) are consistent with a formal charge of +0.5 per et molecule.[1a] The terminal ethylene groups of each molecule are in a staggered conformation when viewed down the molecular long axis. They are ordered, as indicated by their relatively low thermal parameters.

Layers of et molecules and $[Cr(C_2B_9H_{11})_2]^-$ anions alternate along the *c*-direction, as shown in Fig. 2. Each et layer contains stacks of weakly-dimerised et units which extend in the (0 1 0) direction. The interplanar distance between the ttf fragments of the et molecules within each dimer is 3.67 Å and the interdimer separation within the stack is 3.89 Å. Short interstack S···S contacts link adjacent stacks; these interstack S···S distances (3.4–3.6 Å) are markedly shorter than their intrastack counterparts, all of which are longer than 3.7 Å. All of the et molecules in the structure are parallel and are more-or-less

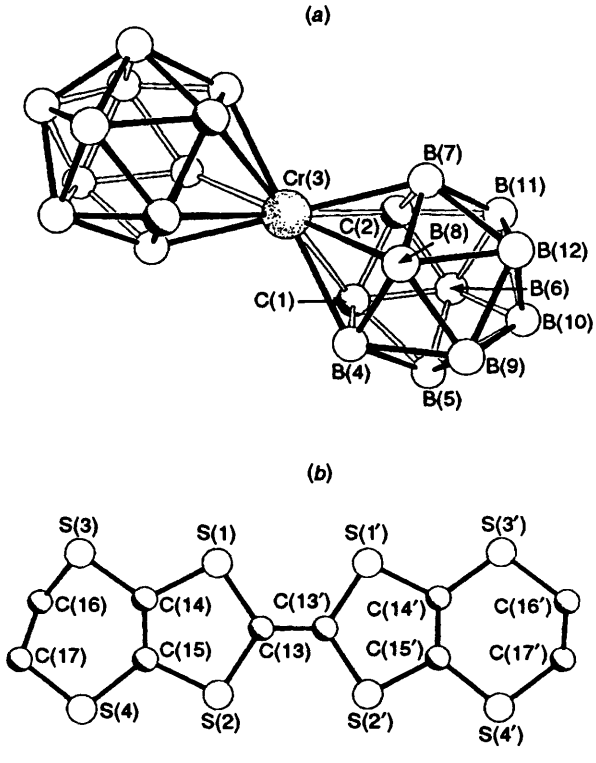

Fig. 1 (*a*) The atomic numbering scheme for the $[Cr(C_2B_9H_{11})_2]^-$ anion in compound **1** (the carbon atoms of the dicarbollide cages are hatched); (*b*) the atomic numbering scheme for the et unit in compound **1**

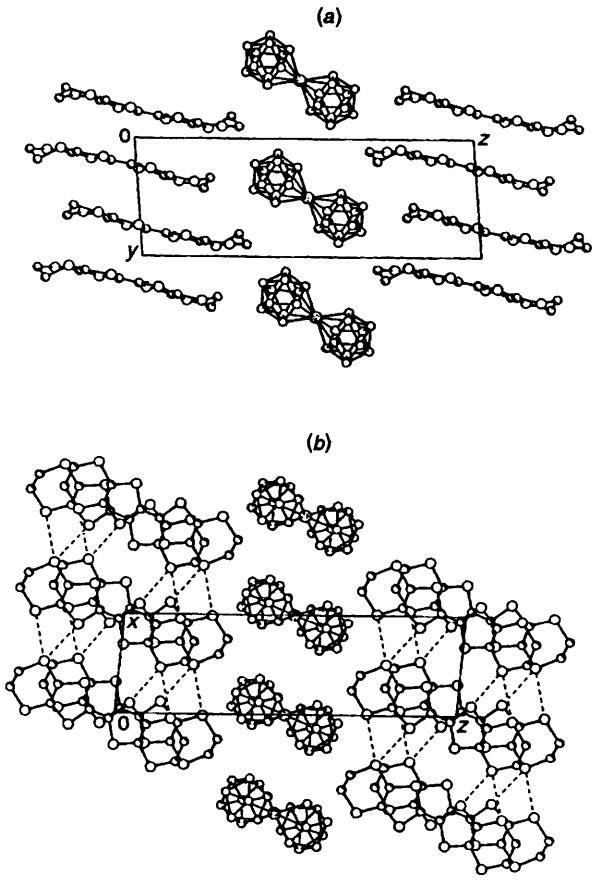

Fig. 2 Packing diagrams for **1**, showing the alternating layers of et units and $[Cr(C_2B_9H_{11})_2]^-$ anions: (*a*) view down the *a*-axis, (*b*) view down the *b*-axis (the dashed lines indicate S···S distances less than 3.7 Å)

Table 1 Selected bond lengths (Å) and angles (°) with estimated standard deviations (e.s.d.s) in parentheses for compound **1**

C(13)–C(13′)	1.367(12)	Cr(3)–C(1)	2.203(11)
C(13)–S(1)	1.740(9)	Cr(3)–C(2)	2.201(9)
C(13)–S(2)	1.737(10)	Cr(3)–B(4)	2.262(10)
C(13′)–S(1′)	1.739(10)	Cr(3)–B(7)	2.207(9)
C(13′)–S(2′)	1.726(9)	Cr(3)–B(8)	2.249(10)
S(1)–C(14)	1.753(9)	C(1)–C(2)	1.640(14)
S(2)–C(15)	1.747(8)	C(1)–B(4)	1.704(14)
S(1′)–C(14′)	1.749(8)	C(2)–B(7)	1.633(15)
S(2′)–C(15′)	1.735(9)	B(4)–B(8)	1.763(17)
C(14)–C(15)	1.342(13)	B(7)–B(8)	1.706(14)
C(14′)–C(15′)	1.344(14)		
C(1)–C(2)–B(7)	110.5(7)	B(5)–B(6)–B(11)	108.6(9)
C(2)–B(7)–B(8)	108.4(8)	B(6)–B(11)–B(12)	108.3(8)
B(4)–B(8)–B(7)	106.7(8)	B(11)–B(12)–B(9)	106.0(9)
C(1)–B(4)–B(8)	104.8(7)	B(12)–B(9)–B(5)	108.6(8)
C(2)–C(1)–B(4)	109.6(8)	B(9)–B(5)–B(6)	108.4(9)

coplanar along the interstack direction, producing the L-type [1a] arrangement shown in Fig. 3. Along the stack the et molecules adopt a modification of the b-mode [1a] of packing, showing small longitudinal offsets between et molecules within the dimers and pronounced sideways displacements, *i.e.* parallel to the short in-plane axes of the et molecules, between dimers. The packing motif of et molecules within the layer thus corresponds to that in the type I β′-$[et]_2X$ salts {X = $[ICl_2]^-$ or $[BrICl]^-$}, which feature a similar stepwise progression of et dimers.[7]

Compound **1** also resembles β′-$[et]_2[ICl_2]$ and β′-$[et]_2$-[BrICl] in the architecture of its unit cell, as shown in Table 2. The most significant difference between the unit cells of **1** and the $[ICl_2]^-$ and $[BrICl]^-$ salts is the length of the *c*-axis. This axis is aligned with the direction of propagation of the alternating cation and anion sheets in all three compounds. The much longer *c*-axis of **1** thus reflects the increased thickness of the anion layers in **1**; this increase is due both to the large size of the anions and the large angles of tilt of the long axes of the anions with respect to the *ab*-plane.

The large size of the $[Cr(C_2B_9H_{11})_2]^-$ anion has the additional effect of increasing the separation between et molecules within the donor layer. This effect is indicated by the distances between unique pairs of et molecules in the layer, as shown in Table 3.

(*ii*) $[et]_2[Fe(C_2B_9H_{10}C_4H_3S)_2]$ **2**. The asymmetric unit of compound **2** comprises two et molecules and one $[Fe(C_2B_9H_{10}C_4H_3S)_2]^-$ anion, the atomic numbering schemes of which are shown in Fig. 4.

Owing to the poor quality of the diffraction data from the crystals of **2** and the rotational disorder of one of the thiophene rings (see Experimental section for more details), the structure of **2** was poorly resolved. The essential features of the structure, however, have been established and an overall analysis of the gross features of the cations and anions and their packing modes is thus considered valid. Specifics of the bonding within the molecules will not be discussed.

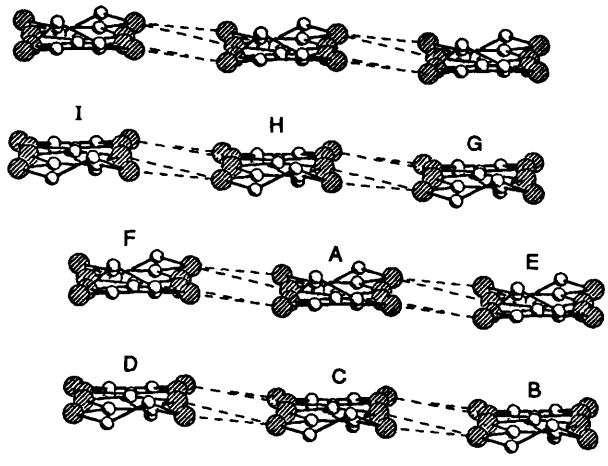

Fig. 3 A single layer of et units in **1**, viewed down the long axes of the molecules, showing the stepwise progression of et dimers

Table 2 Comparison of room-temperature crystallographic data and packing modes for compound **1**, β′-$[et]_2[ICl_2]$ and β′-$[et]_2[BrICl]$[a]

Compound	*a*/Å	*b*/Å	*c*/Å	α/°	β/°	γ/°	*U*/Å^3	(*M*, *S*, *L*)[b]
1	6.634	7.995	21.944	84.05	83.98	76.52	1121.7	(2, 1, 1)
β′-$[et]_2[ICl_2]$	6.645	9.771	12.921	87.19	100.91	98.63	814.3	(2, 1, 1)
β′-$[et]_2[BrICl]$	6.642	9.816	12.975	87.29	101.11	98.28	821.3	(2, 1, 1)

[a] Details in common: space group $P\bar{1}$, $Z = 1$. [b] *M* = Number of et molecules in a single et stack per unit cell, *S* = number of et stacks in one layer of et molecules per unit cell and *L* = number of layers of et molecules in one unit cell; the (*M*, *S*, *L*) values for β′-$[et]_2[ICl_2]$ and β′-$[et]_2[BrICl]$ were taken from ref. 1.

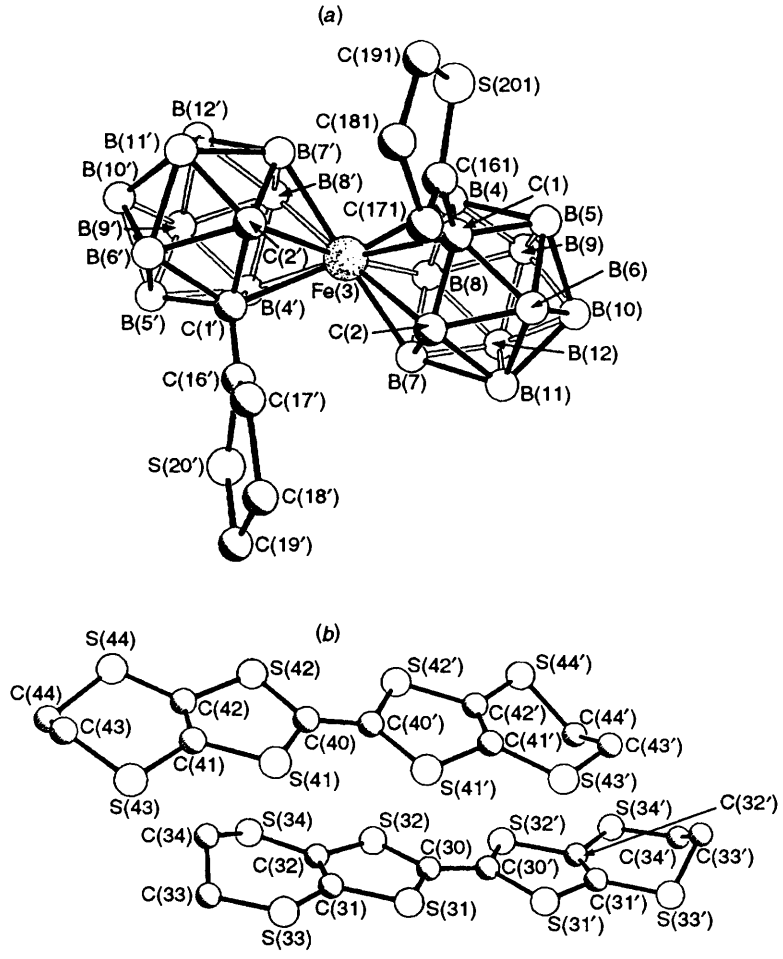

Fig. 4 (*a*) The atomic numbering scheme for the $[Fe(C_2B_9H_{10}C_4H_3S)_2]^-$ anion in compound **2** (the carbon atoms of the dicarbollide cages are hatched). The Fe–C and Fe–B bond lengths are in the ranges 2.09(3)–2.21(3) and 1.92(6)–2.31(5) Å respectively; (*b*) the atomic numbering scheme for the et units in compound **2**

Table 3 Comparison of centroid–centroid[a] distances (Å) between unique pairs of et molecules in compound **1** and β′-$[et]_2[ICl_2]$

	1	β′-$[et]_2[ICl_2]$[b]
A–B[c]	6.63	6.41
A–D	7.29	6.63
A–E	7.17	5.32
A–F	5.12	5.01
A–G	3.88	3.34

[a] As defined by the centroid of the eight sulfur atoms of each et molecule. [b] Values are for the structure determined at 120 K.[1a] [c] See Fig. 3 for the labelling of the et molecules.

In common with most other et salts, compound **2** has a layered structure. This structure, however, is rather unique in that the anions form double layers with all the thiophene groups essentially directed towards each other and away from the et layers, as shown in Fig. 5. This arrangement precludes the occurrence of S · · · S interactions between the et molecules and the thiophene groups. The thickness of the anion layers (*ca.* 12 Å, *cf.* 6 Å for $[et]_2[(NH_4)Hg(SCN)_4]$[11]) also effectively isolates the et layers from each other. There are no short S · · · S contacts between thiophene groups. As the salt crystallises in a centrosymmetric space group, both the DD- and LL-forms of the $[Fe(C_2B_9H_{10}C_4H_3S)_2]^-$ anion are present in the crystals; the *meso* isomer is not observed.

Each donor layer is made up of two crystallographically independent types of et molecules. The ethylene groups are eclipsed in one of these types (hereafter called type X) and staggered in the other (type Y). All of the ethylene groups are ordered. The et molecules are stacked along the (0 0 1) direction, with type X and type Y molecules occurring alternately within the stack. The molecules are engaged in weak pairwise interactions to form dimers (interplanar distances: intradimer 3.7, interdimer 4.0 Å; interplanar angles: intradimer 1, interdimer 16°). Adjacent et molecules along each stack are slipped both longitudinally and sideways with respect to each other. The central C=C bonds of neighbouring molecules are not exactly co-aligned (*ca.* 2° twist). The intrastack packing mode of the et molecules can thus be approximately described as 'a + b'.[1a]

The et molecules adopt the *Z*-mode[1a] of interstack packing, with adjacent stacks being displaced relative to each other along the stacking direction by approximately half the intrastack et · · · et distance. This gives rise to a honeycomb network of interstack S · · · S interactions, as shown in Fig. 6. As usual, the interstack S · · · S contacts (between 3.4 and 3.6 Å) are shorter than the intrastack S · · · S distances (> 3.8 Å).

As in compound **1**, the et molecules in **2** are quite loosely packed, as indicated by their centroid–centroid distances shown in Table 4. The packing in compound **2** is however more isotropic than that in compound **1**. This is reflected in the narrower range of centroid–centroid distances in **2**.

There are no anion–cation distances which are shorter than van der Waals contacts.

(*c*) *Infrared and Optical Spectra.*—An intense, broad charge-

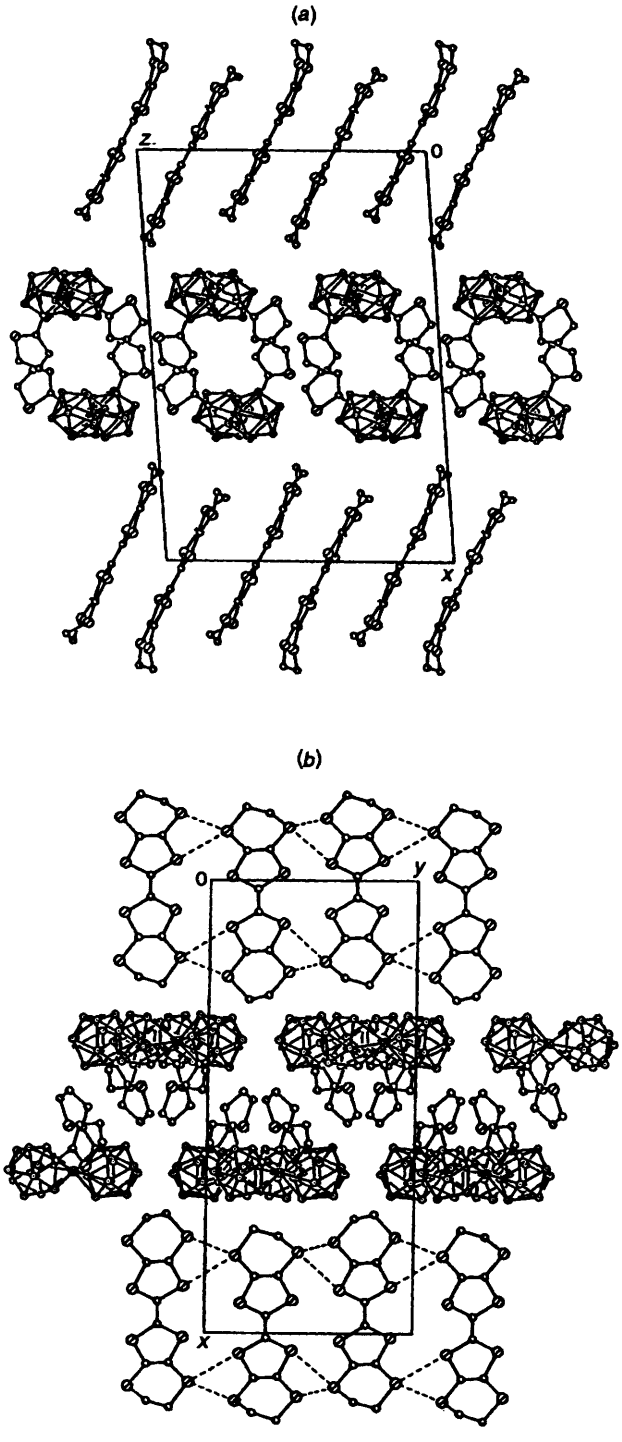

Fig. 5 Packing diagrams for **2**, showing the alternating et single-layers and anion double-layers: (*a*) view down the *b*-axis, (*b*) view down the *c*-axis (the dashed lines indicate S · · · S distances less than 3.7 Å)

Table 4 Selected centroid–centroid[a] distances (Å) between pairs of et molecules in compound **2**

A–B[b]	5.4	B–F	6.6
A–C	6.1	B–G	6.1
A–D	4.0	B–H	5.9
A–E	6.6	B–I	6.8
A–F	6.5	B–J	4.0
A–G	6.5		

[a] As defined by the centroid of the eight sulfur atoms of each et molecule. [b] See Fig. 6 for the labelling of the et molecules.

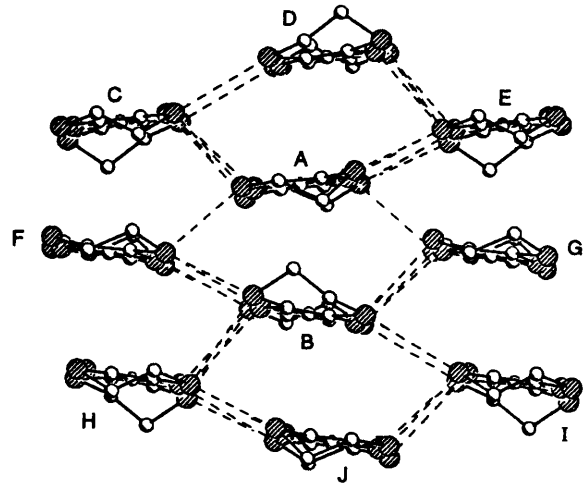

Fig. 6 The honeycomb network of intermolecular S · · · S interactions within a layer of et units in compound **2**

transfer band at *ca.* 4000 cm^{-1} dominates the infrared (IR) spectra of both compounds **1** ($\tilde{\nu}_{max}$ 4400 cm^{-1}) and **2** ($\tilde{\nu}_{max}$ 4200 cm^{-1}) (as KBr pellets). The presence of this electronic band (band A in the notation of Torrance *et al.*[12]) is consistent with the average charge of +0.5 on the et molecules in compounds **1** and **2**. It does not, however, indicate whether the valence electrons are equally delocalised over all the et molecules ('mono-valence' configuration) or are localised on individual molecules, with the crystal lattice containing equal numbers of $[et]^0$ and $[et]^+$ molecules ('mixed-valence' configuration). The vibronic region of each IR spectrum (1400–1200 cm^{-1}) features two very intense broad absorptions (at 1348 and 1274 cm^{-1} for **1** and 1343 and 1284 cm^{-1} for **2**) which are assigned to the totally symmetric stretchings of the central and ring C=C bonds of the et molecules.[13] The high intensities of these a_g bands result from vibronic coupling of the molecular vibrations with the charge-transfer transitions between the et molecules.[13] In the spectrum of compound **2**, an additional strong absorption band occurs at 1407 cm^{-1}, which is attributed to the –C–C–H bending vibrations of the ethylene groups of the et molecules.[13] The unusually high intensity of this absorption could be due to strong coupling between the bending mode and the vibronic transitions.[13] The intense, broad bands due to the B–H stretching absorptions of the metallacarborane anions in compounds **1** and **2** are centred at *ca.* 2525 and 2548 cm^{-1} respectively.

The optical spectra of both compounds **1** and **2** (as KBr pellets) exhibit a prominent band at *ca.* 10 600 cm^{-1} (940 nm). This band, labelled 'B' by Torrance *et al.*,[12] is attributed to charge-transfer transitions between singly-charged $[et]^+$ cations, *i.e.* $\{[et]^+, [et]^+\} \longrightarrow \{[et]^0, [et]^{2+}\}$.[12] The relatively high intensity of band B in the spectra of **1** and **2** thus suggests the presence of $[et]^+$ molecules in compounds **1** and **2**, and hence the adoption of mixed-valence configurations by compounds **1** and **2**. A mixed-valence et salt is expected to contain et molecules with different geometries corresponding to their different charges. The fact that the et molecules in compound **1** are all crystallographically equivalent can be explained by noting that the single-crystal X-ray diffraction experiment provides a time-averaged structure if the crystal structure being studied is fluxional on the time-scale of the experiment. Some charge-transfer salts of ttf and tetrathianaphthacene which are apparently mono-valent within the time-scale of X-ray crystallography[14] have been found to have mixed-valence configurations within the time-scale of X-ray photoelectron spectroscopy.[15]

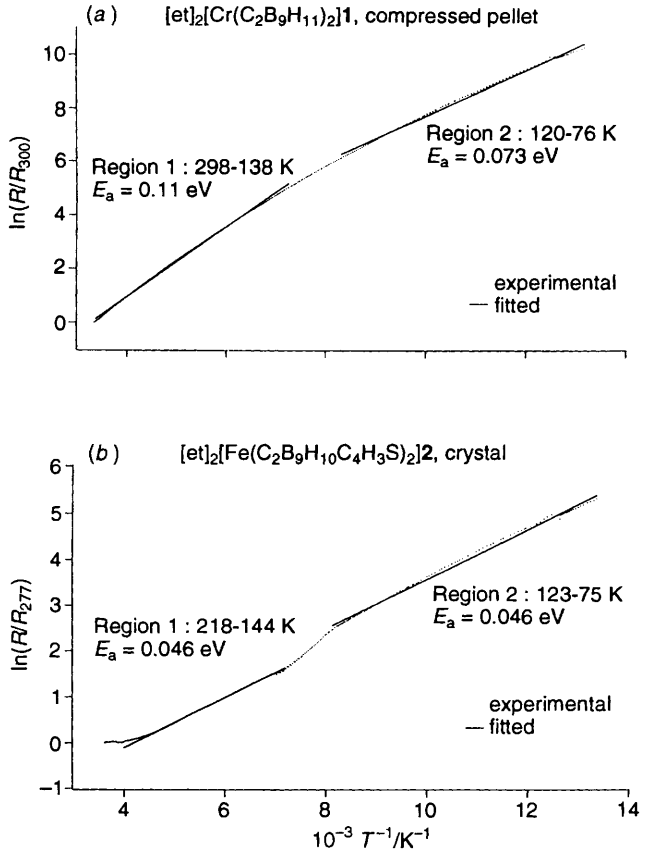

Fig. 7 (*a*) Plot of ln (R/R_{300}) *vs.* reciprocal temperature for **1**; (*b*) plot of ln (R/R_{277}) *vs.* reciprocal temperature for **2**

(*d*) *Electrical Conductivity.*—Compound **1** (as a compressed pellet) has a room-temperature electrical conductivity of *ca.* 2×10^{-3} S cm^{-1}. Variable-temperature resistance measurements (300–76 K) show that the conductivity of compound **1** is thermally activated. The resistance data cannot, however, be fitted with the simple exponential law, $R \propto \exp(E_a/kT)$, with constant activation energy E_a. A plot of the natural logarithm of the normalized resistance of compound **1** *vs.* reciprocal temperature is shown in Fig. 7(*a*). The high- and low-temperature regions of the plot could be separately fitted with the exponential law to yield activation energies of 0.11 and 0.073 eV respectively.

The conductivity of crystals of compound **2** at room temperature is *ca.* 0.5 S cm^{-1}. The resistance of the crystals exhibits complex temperature dependence, as shown in Fig. 7(*b*). Data points for temperatures higher than 277 K are not shown because these data were not reproducible between different crystals and measurements. Two main semiconducting regions are observed, both of which have a low activation energy of 0.046 eV. The higher *y*-intercept of the fitted line for region 2 corresponds to a larger proportionality constant *A* in the exponential function $R = A \exp(E_a/kT)$. Since the constant *A* is a measure of the mobility of the conduction electrons (larger *A* indicates lower mobility), the higher *y*-intercept value for region 2 suggests that the conduction electrons are less mobile in region 2.

The gradient of the plot of ln (R/R_{277}) *vs.* T^{-1} for compound **2** decreases gradually above 218 K and becomes nearly zero above *ca.* 250 K. This suggests that compound **2** undergoes a gradual transition to a pseudo-metallic state above 218 K. Crystals of higher quality are required for a thorough investigation of the temperature dependence of the conductivity of compound **2** above 277 K.

The relatively loose packing of the et molecules in compounds **1** and **2** is expected to result in electronic bands with narrow bandwidths. Low-dimensional molecular conductors with narrow bandwidths are more unstable towards localisation of conduction electrons and are therefore more likely to be non-metallic.[16] The semiconducting behaviours of compounds **1** and **2** are thus consistent with the nature of their molecular packing, especially for compound **1**, which has a more anisotropic arrangement of et molecules. This anisotropic character is expected to give rise to a one-dimensional band structure, thus making compound **1** more unstable towards a high-temperature metal-to-insulator transition.[16,17]

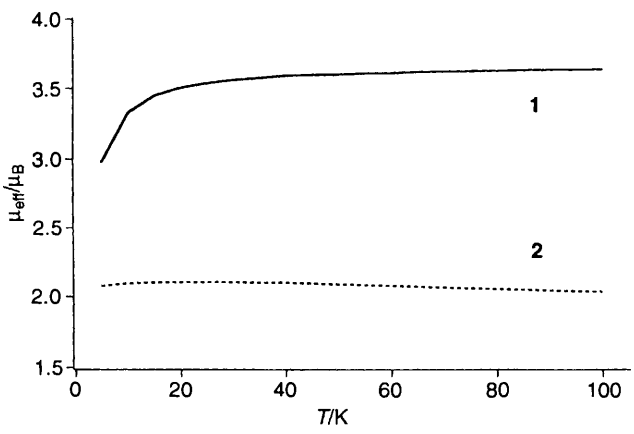

Fig. 8 Plots of μ_{eff} *vs.* temperature (5–100 K) for compounds **1** and **2**

(*e*) *Magnetic Properties.*—Between 25 and 300 K the corrected molar magnetic susceptibilities of compounds **1** and **2** follow the Curie–Weiss law, $\chi = C/(T - \theta)$, with θ values of -1.1 and $+1.6$ K respectively. The θ values indicate the presence of weak antiferromagnetic interactions in **1** and that of weak ferromagnetic interactions in **2**. The effective moments μ_{eff} $[= (8\chi T)^{\frac{1}{2}}]$ of the compounds are nearly independent of temperature between 25 and 300 K. The average moments μ_{av} $[= (8C)^{\frac{1}{2}}]$ of compounds **1** and **2** between 25 and 300 K are 3.6 and 2.0 μ_B respectively. These values are very close to those of $Cs[Cr(C_2B_9H_{11})_2]$ (3.8 μ_B)[18] and $[NMe_4][Fe(C_2B_9H_{11})_2]$ (2.1 μ_B)[19] respectively. There is thus apparently no contribution from the et cation-radicals to the bulk magnetic susceptibilities of compounds **1** and **2**. A similar situation has been observed in $[et]_2[FeCl_4]$.[20] Below 25 K the μ_{eff} of compound **1** begins to decrease appreciably, reaching a value of 3.0 μ_B at 5 K, whilst that of compound **2** increases gradually to a maximum value of 2.1 μ_B at 10 K (see Fig. 8).

The shortest metal–metal (M ··· M) distances in compounds **1** and **2** are 6.6 and 9.2 Å respectively. Since the magnetic orbitals are primarily localised on the metal atoms in metallacarborane complexes,[21] the long M ··· M distances preclude strong magnetic interactions between the spins in compounds **1** and **2**.

Conclusion

This study has shown that it is possible to synthesise a single phase of the cation-radical salt $[et]_2[Cr(C_2B_9H_{11})_2]$ **1** in moderate yields by chemical oxidation. In principle, the synthetic strategy can be used to synthesise other cation-radical salts, provided the conjugate acid of the anion is a strong acid and is available. Compound **1** is structurally very similar to the type I β′-$[et]_2X$ salts {X = $[ICl_2]^-$ or $[BrICl]^-$} and hence can be classified as a magnetic analogue of the latter. The adoption of the type I structure by the chromacarborane salt also suggests that the packing of et molecules in this salt is determined more by the prolateness of the anion than by the length of the anion. The structure of the ferracarborane salt $[et]_2[Fe(C_2B_9H_{10}C_4H_3S)_2]$ **2** indicates that inter-et S ··· S

interactions are favoured over et-thiophene S • • • S interactions. The anions thus pack to form double layers in which the thiophene groups are oriented towards each other and away from the et layers and are intermeshed for more efficient packing. The weak ferromagnetic coupling observed in **2**, together with the ferromagnetic coupling observed in $[ttf]_5[Fe(C_2B_9H_{10}C_4H_3S)_2]_2$ and $[ttf][Fe(C_2B_9H_{10}C_4H_3S)_2]$,[8b] suggests that the $[Fe(C_2B_9H_{10}C_4H_3S)_2]^-$ anion favours ferromagnetic interactions in its cation-radical salts. Both compounds **1** and **2** are semiconductors with low activation energies and complex temperature-dependent conductivities in the temperature ranges studied. The absence of metallic behaviour may be attributed in part to the loose packing of the et molecules, due to the large size of the anions, in compounds **1** and **2**.

Experimental

(*a*) *General.*—The commercially available compounds bis(ethylenedithio)tetrathiafulvalene (Fluka) and 2,3-dichloro-5,6-dicyano-*p*-benzoquinone (Aldrich) were used without further purification. Technical grade *p*-benzoquinone (BDH) was vacuum-sublimed before use. The compound $Cs[Cr(C_2B_9H_{11})_2]$ was prepared by the literature method[18] and $[NBu^n_4][Fe(C_2B_9H_{10}C_4H_3S)_2]$ was synthesised as previously described.[8b] Dry 1,1,2-trichloroethane used for the electrocrystallisation experiments was obtained from Aldrich in a SureSeal™ bottle and used as received. The other organic solvents used were of reagent grade and were dried by published procedures[22] and distilled under nitrogen. Reactions were routinely carried out under nitrogen using standard Schlenk techniques.

(*b*) *Physical Measurements.*—Infrared spectra in the 5000–220 cm^{-1} region were recorded on a Perkin-Elmer 1720 Fourier-transform spectrometer and optical spectra were obtained using a Perkin-Elmer Lambda 2 UV/VIS spectrophotometer. Near-infrared spectra in the 10 000–3000 cm^{-1} region were obtained on a Perkin-Elmer 1760X FT-IR spectrometer.

Magnetic susceptibility measurements were performed in the range $5 \leqslant T \leqslant 300$ K using a Quantum Design MPMS-7 SQUID magnetometer under a magnetic field strength of 0.4 T. Microcrystalline samples were loaded in gelatin capsules and then fixed in plastic straws. The magnetic susceptibilities were corrected for the temperature-independent contributions from the sample and capsule by fitting the susceptibility data by the expression $\chi^{-1} = (T - \theta)[C + k(T - \theta)]^{-1}$, where k comprises the total diamagnetism and any temperature-independent paramagnetism of the sample and capsule.

Electrical conductivity measurements were carried out on a compressed pellet of compound **1** and on crystals of compound **2**, using the two-probe d.c. method. Contacts were made with platinum paint and 25 μm gold wires.

(*c*) *Synthesis of* $[et]_2[Cr(C_2B_9H_{11})_2]$ **1**.—(*i*) *By hydrogen peroxide oxidation.* A solution of $Cs[Cr(C_2B_9H_{11})_2]$ (0.056 g,

Table 5 Crystal and refinement data for compounds **1** and **2**

Compound	**1**	**2**
(*a*) Crystal data		
Chemical formula	$C_{24}H_{38}B_{18}CrS_{16}$	$C_{32}H_{42}B_{18}FeS_{18}$
M	1086.1	1254.2
Crystal system	Triclinic	Monoclinic
Unit cell dimensions:		
a/Å	6.634(2)	25.748(12)
b/Å	7.995(2)	11.638(6)
c/Å	21.944(5)	17.717(7)
α/°	84.05(2)	90
β/°	83.98(2)	94.88(2)
γ/°	76.52(2)	90
U/Å^3	1121.7(4)	5289(5)
Space group	$P\bar{1}$	$P2_1/c$
D_c/g cm^{-3}	1.608	1.575
Z	1	4
F(000)	552	2552
Colour, habit	Bronze needles	Black plates
Crystal dimensions/mm	0.008 × 0.047 × 0.141	0.48 × 0.19 × 0.05
μ/cm^{-1}	92.5 (Cu-Kα)	10.3 (Mo-Kα)
(*b*) Data collection and processing		
Diffractometer	Siemens P4/RA	Siemens P4/PC
X-radiation (λ/Å)	Cu-Kα (1.541 78)	Mo-Kα (0.710 73)
Scan mode	ω	ω
Scan width/°	0.90	1.20
2θ limits/°	3.0–125.0	7.0–45.0
No. of reflections:		
Total	3587	5133
Unique (R_{int}/%)	3587 (0.00)	4916 (7.05)
Observed	2276 [$F > 6.0\sigma(F)$]	2192 [$F > 3.0\sigma(F)$]
Absorption correction	Face-indexed numerical	None
Min., max. transmissions	0.4814, 0.9297	
(*c*) Structural analysis and refinement		
No. of parameters	271	383
Weighting scheme, w^{-1}	$\sigma^2(F) + 0.0009F^2$	$\sigma^2(F) + 0.0009F^2$
R (observed data)[a]	0.0607	0.1341
R' (observed data)[b]	0.0666	0.1276

[a] $R = \Sigma(|F_o| - |F_c|)/\Sigma|F_o|$. [b] $R' = [\Sigma w(|F_o| - |F_c|)^2/\Sigma w|F_o|^2]^{\frac{1}{2}}$.

0.12 mmol) in acetone (*ca.* 10 cm^3) was loaded onto a column (2.4 × 8 cm) of Dowex 50 cation-exchange resin (H^+ form) and the column was eluted with acetone. The $H[Cr(C_2B_9H_{11})_2]$-containing aliquot was evaporated to dryness under reduced pressure and the residue was redissolved in thf (*ca.* 70 cm^3) together with et (0.095 g, 0.25 mmol). A 0.077 g amount of an aqueous solution of H_2O_2 (27.5% w/w) was diluted to 10.0 cm^3 with thf in a volumetric flask. A 1.0 cm^3 amount of the diluted solution (equivalent to 2.1 mg H_2O_2, 0.062 mmol) was then added dropwise from a graduated pipette to the magnetically stirred solution of et and $H[Cr(C_2B_9H_{11})_2]$ at room temperature. The solution turned from orange to dark red-violet and shiny bronze-coloured needles of $[et]_2[Cr(C_2B_9H_{11})_2]$ **1** slowly precipitated. The mixture was stirred at room temperature for 40 min and then filtered to give 0.032 g (25% yield) of compound **1** (Found: C, 26.9; H, 3.3. $C_{24}H_{38}B_{18}CrS_{16}$ requires C, 26.5; H, 3.5%); $\tilde{\nu}_{max}/cm^{-1}$ 2544s (br) and 2506s (br) (BH), 1456m, 1408m, 1348vs (br), 1288s, 1274vs (br), 1016w, 968m, 882m, 646m, 458s, 436s, 386s (KBr).

(*ii*) *By* p-*benzoquinone oxidation.* The salt $Cs[Cr(C_2B_9H_{11})_2]$ (0.019 g, 0.042 mmol) was ion-exchanged to the acid as described above. The $H[Cr(C_2B_9H_{11})_2]$ intermediate was dissolved in thf (25 cm^3) together with et (0.032 g, 0.083 mmol). A solution of *p*-benzoquinone (2.5 mg, 0.023 mmol) in thf (6 cm^3) was then transferred to the agitated et–$H[Cr(C_2B_9H_{11})_2]$ solution. The solution turned deep violet immediately and needles of compound **1** slowly precipitated (*ca.* 5 min). The mixture was left undisturbed overnight at 21 °C and then filtered to isolate the crystals. Yield: 0.019 g (42%) (Found: C, 26.8; H, 2.9%). The IR spectrum of the product is identical to that given above.

(*iii*) *By* ddq *oxidation.* The procedure was very similar to that described for the *p*-benzoquinone oxidation except that the crystals were isolated after 2 h instead of after having left the mixture overnight. The yield of compound **1** was 52%. The IR spectrum of the product is identical to that given above.

(*d*) *Synthesis of* $[et]_2[Fe(C_2B_9H_{10}C_4H_3S)_2]$ **2**.—The electrocrystallisation [1,23] of compound **2** was carried out in a two-compartment H-cell fitted with a nitrogen inlet. The anode and cathode compartments, which were separated by a fine-porosity glass frit, were initially sealed with rubber septa. A solution of et (0.010 g, 0.026 mmol) in 1,1,2-trichloroethane (3.3 cm^3) was first syringed into the anode compartment. A 5 cm^3 portion of a solution of $[NBu^n_4][Fe(C_2B_9H_{10}C_4H_3S)_2]$ (0.454 g, 0.62 mmol) in 1,1,2-trichloroethane (6.7 cm^3) was then added to the cathode compartment; the remaining 1.7 cm^3 of the solution were added to the anode compartment. The rubber septa were then replaced with platinum wire electrodes and a current of *ca.* 2 μA cm^{-2} was applied using a constant-current source. The H-cell was shielded from direct light to avoid possible photochemical decomposition of et. Black platelets of compound **2** were harvested from the bottom of the anode compartment after 2–4 weeks (Found: C, 30.6; H, 3.1. $C_{32}H_{42}B_{18}FeS_{18}$ requires C, 30.6; H, 3.4%); $\tilde{\nu}_{max}/cm^{-1}$ 2548vs (br) (BH), 1407vs, 1343vs (br), 1284vs (br), 1171m, 988m, 880m, 697m, 475m, 454m, 435m (KBr).

(*e*) *X-Ray Crystallography.*—The crystal and refinement data for compounds **1** and **2** are summarised in Table 5, atomic coordinates are given in Tables 6 and 7.

The crystal of compound **1** used for data collection was selected from the sample prepared by *p*-benzoquinone oxidation. Owing to the exceptionally small size of the crystals available, data were collected using a rotating anode X-ray source with Cu-Kα radiation. The crystal structure was solved by direct methods and refined by the full-matrix least-squares method. Cage carbon atoms of the $[Cr(C_2B_9H_{11})_2]^-$ anion were identified by their low isotropic thermal parameters after refinement as boron atoms. Anomalously short C(2)–B(7), B(7)–B(8) and Cr(3)–B(7) bond lengths were observed, indicating a possible rotational disorder of the chromacarborane anion and/or the dicarbollide cages about the molecular long axis which exchanges the C(1) and B(7) positions. However, refinement of the structure with the C(1) and B(7) sites assigned mixed C and B occupancies (50:50) did not improve the agreement factor. However, the exact nature of the 1, 2 and 7 sites cannot be definitively assigned. After anisotropic refinement of the non-hydrogen atoms, the hydrogen atoms of the et molecule were introduced in calculated positions and refined isotropically. Those on the dicarbollide cage were located by difference syntheses and refined with the bond length constraints C–H 0.960 ± 0.002 and B–H 1.080 ± 0.002 Å and assigned isotropic thermal parameters $U(H) = 1.2\ U_{eq}(C, B)$. Calculations were performed on 486 personal computers using the PC version of the SHELXTL PLUS software package.[24]

Table 6 Atomic coordinates (× 10^4) with e.s.d.s in parentheses for compound **1**

Atom	*x*	*y*	*z*
Cr(3)	0	−5 000	5 000
C(1)	646(16)	−2 884(12)	5 461(4)
C(2)	−1 728(14)	−2 424(12)	5 245(4)
B(4)	1 027(17)	−4 747(14)	5 931(4)
B(5)	479(20)	−2 701(15)	6 244(5)
B(6)	−1 238(21)	−1 226(15)	5 794(5)
B(7)	−2 953(15)	−3 918(14)	5 528(5)
B(8)	−1 341(17)	−5 413(15)	5 974(4)
B(9)	−792(17)	−4 325(15)	6 585(5)
B(10)	−2 153(17)	−2 166(14)	6 488(5)
B(11)	−3 564(17)	−1 913(15)	5 829(5)
B(12)	−3 331(18)	−3 870(16)	6 338(5)
S(1)	−2 976(3)	−1 615(4)	10 957(1)
S(1′)	−1 000(4)	−2 561(4)	9 587(1)
S(2)	1 192(3)	−1 753(4)	11 315(1)
S(2′)	3 143(4)	−2 598(4)	9 945(1)
S(3)	−5 079(3)	−882(4)	12 188(1)
S(3′)	481(4)	−3 655(4)	8 338(1)
S(4)	−131(4)	−1 050(4)	12 600(1)
S(4′)	5 386(4)	−3 636(5)	8 783(1)
C(13)	−327(14)	−1 925(13)	10 736(4)
C(13′)	507(14)	−2 267(13)	10 153(4)
C(14)	−2 783(13)	−1 243(12)	11 719(4)
C(14′)	1 094(13)	−3 177(12)	9 042(4)
C(15)	−870(13)	−1 309(12)	11 882(4)
C(15′)	2 981(15)	−3 192(13)	9 216(4)
C(16)	−4 024(15)	−1 904(13)	12 898(4)
C(16′)	2 771(17)	−3 351(15)	7 861(4)
C(17)	−2 477(15)	−1 030(13)	13 106(4)
C(17′)	4 785(18)	−4 242(18)	8 070(5)

Compound **2** crystallises as very thin, small, slightly corrugated plates. Several crystals were investigated, all of which gave diffuse diffraction patterns. Fairly wide scan widths were thus used but despite this the quality of the diffraction data from the chosen crystal was poor. The percentage of observed data was also severely limited.

The crystal structure of compound **2** was solved by direct methods. In the initial cycles of full-matrix least-squares refinement, only the iron and sulfur atoms were refined anisotropically, and the bond lengths within the dicarbollide cages, the et molecules and the thiophene rings were constrained to vary within ±0.03, ±0.05 and ±0.01 Å, respectively, of idealised values. Although the position of one of the carbon atoms in each carborane cage is defined by the bonding of the thiophene ring, the other can be difficult to assign with confidence. Here the other carbon atom in each cage was assigned on the basis of the bond lengths and thermal parameters. However, within the limits of accuracy of this structure determination the possibility of C(2)/B(4) and

Table 7 Atomic coordinates ($\times 10^4$) with e.s.d.s in parentheses for compound 7

Atom	*x*	*y*	*z*	Atom	*x*	*y*	*z*
Fe(3)	3549(2)	6495(5)	2834(3)	S(31′)	−1028(3)	6055(8)	−117(6)
C(1)	4039(12)	5408(30)	3630(21)	S(32′)	−949(3)	8540(10)	−334(6)
C(2)	3953(15)	4923(33)	2802(24)	S(33′)	−2119(4)	5881(9)	−822(7)
B(4)	3424(16)	5887(44)	3942(28)	S(34′)	−2006(3)	8825(9)	−1095(7)
B(5)	3769(15)	4506(38)	4265(27)	C(40)	372(9)	7047(14)	3523(17)
B(6)	4099(19)	4031(43)	3628(28)	C(41)	1262(8)	6480(16)	4180(19)
B(7)	3376(21)	4919(49)	2612(37)	C(42)	1248(8)	7631(16)	4226(18)
B(8)	2970(15)	5335(35)	3160(23)	C(43)	2140(10)	6541(21)	5006(15)
B(9)	3096(18)	4496(40)	3970(28)	C(44)	2287(9)	7704(23)	4737(23)
B(10)	3505(19)	3392(54)	3832(32)	S(41)	721(3)	5795(9)	3721(6)
B(11)	3668(16)	3495(46)	2822(29)	S(42)	659(3)	8287(9)	3900(6)
B(12)	3037(17)	3935(39)	3090(26)	S(43)	1785(4)	5558(9)	4413(6)
C(1′)	3772(13)	7276(32)	1829(22)	S(44)	1706(4)	8566(9)	4658(7)
C(2′)	4065(12)	7801(27)	2585(19)	C(40′)	−106(9)	7049(14)	3086(16)
B(4′)	3121(15)	7376(36)	1932(24)	C(41′)	−970(8)	6456(17)	2358(19)
B(5′)	3443(15)	8444(39)	1340(28)	C(42′)	−996(8)	7602(16)	2429(19)
B(6′)	4063(17)	8739(41)	1733(27)	C(43′)	−1942(9)	6465(21)	1552(19)
B(7′)	3688(16)	8169(37)	3158(28)	C(44′)	−1771(11)	7639(21)	1334(13)
B(8′)	3054(19)	8147(40)	2831(29)	S(41′)	−387(3)	5803(9)	2722(7)
B(9′)	2986(16)	8699(39)	1976(25)	S(42′)	−458(4)	8298(9)	2908(7)
B(10′)	3561(16)	9728(44)	1941(29)	S(43′)	−1415(4)	5520(8)	1886(7)
B(11′)	3987(15)	9295(37)	2675(25)	S(44′)	−1515(3)	8485(9)	2133(6)
B(12′)	3344(17)	9368(44)	2829(28)	C(16′)	4022(9)	6476(30)	1346(14)
C(30)	−194(8)	7299(14)	481(17)	C(17′)	4561(8)	6173(29)	1377(17)
C(31)	672(8)	6695(16)	1201(17)	C(18′)	4606(10)	5317(31)	815(21)
C(32)	702(8)	7834(16)	1143(17)	C(19′)	4178(10)	5192(35)	258(18)
C(33)	1666(9)	6660(24)	1898(21)	S(20′)	3672(4)	5926(15)	575(7)
C(34)	1534(14)	7807(24)	2197(17)	C(16)	4520(8)	6019(27)	3939(14)
S(31)	98(3)	6041(8)	819(6)	C(17)*	4950(17)	6194(59)	3500(22)
S(32)	182(3)	8522(9)	629(6)	C(18)*	5347(12)	6636(68)	4024(36)
S(33)	1105(4)	5750(9)	1692(6)	C(19)*	5188(14)	7244(63)	4658(32)
S(34)	1203(3)	8728(9)	1500(6)	S(20)*	4567(8)	6819(36)	4738(15)
C(30′)	−683(9)	7309(14)	65(17)	C(171)*	4568(24)	6702(78)	4607(37)
C(31′)	−1572(8)	6744(17)	−579(19)	C(181)*	5064(23)	7242(81)	4651(36)
C(32′)	−1530(8)	7873(16)	−707(19)	C(191)*	5383(12)	7020(44)	4052(31)
C(33′)	−2630(9)	6908(21)	−739(17)	S(201)*	5074(6)	6016(26)	3489(12)
C(34′)	−2549(12)	7899(29)	−1240(23)				

* Occupancy 0.5.

C(2′)/B(4′) reversal cannot be totally ruled out. In the initial stages of refinement the sulfur atom S(201) and the β-carbon atom C(171) of one thiophene ring had relatively high and low isotropic thermal parameters respectively. This was attributed to disorder in the ring corresponding to a 180° rotation about the C(1)–C(161) bond. An occupancy refinement indicated a 50% rotational disorder. The thiophene ring geometries were optimised and the rings refined isotropically subject to C–C and C–S distance constraints of 1.42 ± 0.02 and 1.69 ± 0.02 Å respectively. Hydrogen atoms of the et molecules and those of the thiophene rings [C(161)–S(201)] and [C(16′)–S(20′)] were introduced in idealised positions using the built-in function of the SHELXTL PLUS software package. The positions of the hydrogen atoms on the metallacarborane cages were calculated by taking the vectors joining the pairs of diametrically opposite vertices within each icosahedral fragment and extending each vector in opposite directions by amounts corresponding to the C–H (0.96 Å) or B–H (1.08 Å) bond lengths. The hydrogen atoms were allowed to ride on the carbon/boron atoms. Owing to the limited number of observed data (a 3σ cut off was used to try and improve this) only the Fe and the full occupancy S atoms were refined anisotropically.

Additional material available from the Cambridge Crystallographic Data Centre comprises H-atom coordinates, thermal parameters and remaining bond lengths and angles.

Acknowledgements

Support of this work by the EPSRC is acknowledged. Y.-K. Y. thanks the Nanyang Technological University, Singapore, for a scholarship and D. M. P. M. thanks B.P. for a generous endowment. We are also grateful to Professor J. D. Woollins, University of Loughborough, for the loan of his electrocrystallisation apparatus.

References

1 (*a*) J. M. Williams, H. H. Wang, T. J. Emge, U. Geiser, M. A. Beno, P. C. W. Leung, K. D. Carlson, R. J. Thorn, A. J. Schultz and M.-H. Whangbo, *Prog. Inorg. Chem.*, 1987, **35**, 51; (*b*) J. M. Williams, J. R. Ferraro, R. J. Thorn, K. D. Carlson, U. Geiser, H. H. Wang, A. M. Kini and M.-H. Whangbo, *Organic Superconductors (including Fullerenes): Synthesis, Structure, Properties and Theory*, Prentice Hall, Englewood Cliffs, NJ, 1992; (*c*) Proceedings of the International Conference on Synthetic Metals 1992, *Synth. Met.*, 1993, **56**.

2 M.-H. Whangbo, J. M. Williams, A. J. Schultz, T. J. Emge and M. A. Beno, *J. Am. Chem. Soc.*, 1987, **109**, 90; J. J. Novoa, M.-H. Whangbo and J. M. Williams, *Mol. Cryst. Liq. Cryst.*, 1990, **181**, 25; M.-H. Whangbo, J. J. Novoa, D. Jung, J. M. Williams, A. M. Kini, H. H. Wang, U. Geiser, M. A. Beno and K. D. Carlson, in *Organic Superconductivity*, eds. V. Z. Kresin and W. A. Little, Plenum, New York, 1990, p. 243.

3 K. Murata, M. Tokumoto, H. Anzai, H. Bando, G. Saito, K. Kajimura and T. Ishiguro, *J. Phys. Soc. Jpn.*, 1985, **54**, 2084; J. E. Schirber, L. J. Azevedo, J. F. Kwak, E. L. Venturini, P. C. W. Leung, M. A. Beno, H. H. Wang and J. M. Williams, *Phys. Rev. B.*, 1986, **33**, 1987; J. E. Schirber, J. F. Kwak, M. A. Beno, H. H. Wang and J. M. Williams, *Physica B (Amsterdam)*, 1986, **143**, 343.

4 H. H. Wang, M. A. Beno, U. Geiser, M. A. Firestone, K. S. Webb, L. Nuñez, G. W. Crabtree, K. D. Carlson, J. M. Williams, L. J. Azevedo, J. F. Kwak and J. E. Schirber, *Inorg. Chem.*, 1985, **24**, 2465.

5 J. M. Williams, H. H. Wang, M. A. Beno, T. J. Emge, L. M. Sowa, P. T. Copps, F. Behroozi, L. N. Hall, K. D. Carlson and G. W. Crabtree, *Inorg. Chem.*, 1984, **23**, 3839.
6 M. Tokumoto, H. Anzai, T. Ishiguro, G. Saito, H. Kobayashi, R. Kato and A. Kobayashi, *Synth. Met.*, 1987, **19**, 215; see ref. 1(*b*), ch. 4, p. 131.
7 T. J. Emge, H. H. Wang, P. C. W. Leung, P. R. Rust, J. D. Cook, P. L. Jackson, K. D. Carlson, J. M. Williams, M.-H. Whangbo, E. L. Venturini, J. E. Schirber, L. J. Azevedo and J. R. Ferraro, *J. Am. Chem. Soc.*, 1986, **108**, 695.
8 (*a*) J. M. Forward, D. M. P. Mingos, T. E. Müller, D. J. Williams and Y.-K. Yan, *J. Organomet. Chem.*, 1994, **467**, 207; (*b*) Y.-K. Yan, D. M. P. Mingos, M. Kurmoo, W.-S. Li, I. J. Scowen, M. McPartlin, A. T. Coomber and R. H. Friend, *J. Chem. Soc., Dalton Trans.*, 1995, 2851.
9 P. Day, *Chem. Soc. Rev.*, 1993, 51; T. Mori and H. Inokuchi, *Bull. Chem. Soc. Jpn.*, 1988, **61**, 591; P. Day, M. Kurmoo, T. Mallah, I. R. Marsden, R. H. Friend, F. L. Pratt, W. Hayes, D. Chasseau, J. Gaultier, G. Bravic and L. Ducasse, *J. Am. Chem. Soc.*, 1992, **114**, 10 722; I. R. Marsden, M. L. Allan, R. H. Friend, M. Kurmoo, D. Kanazawa, P. Day, G. Bravic, D. Chasseau, L. Ducasse and W. Hayes, *Phys. Rev. B*, 1994, **50**, 2118.
10 M. Kurmoo, D. R. Talham, P. Day, J. A. K. Howard, A. M. Stringer, D. S. Obertelli and R. H. Friend, *Synth. Met.*, 1988, **22**, 415.
11 H. Mori, S. Tanaka, M. Oshima, G. Saito, T. Mori, Y. Maruyama and H. Inokuchi, *Bull. Chem. Soc. Jpn.*, 1990, **63**, 2183.
12 J. B. Torrance, B. A. Scott, B. Welber, F. B. Kaufman and P. E. Seiden, *Phys. Rev. B*, 1979, **19**, 730.
13 M. E. Kozlov, K. I. Pokhodnia and A. A. Yurchenko, *Spectrochim. Acta, Part A*, 1989, **45**, 437.
14 T. J. Kistenmacher, T. E. Phillips and D. O. Cowan, *Acta Crystallogr., Sect. B*, 1974, **30**, 763; B. A. Scott, S. J. La Placa, J. B. Torrance, B. D. Silverman and B. Welber, *J. Am. Chem. Soc.*, 1977, **99**, 6631; D. L. Smith and H. R. Luss, *Acta Crystallogr., Sect. B*, 1977, **33**, 1744.
15 I. Ikemoto, M. Yamada, T. Sugano and H. Kuroda, *Bull. Chem. Soc. Jpn.*, 1980, **53**, 1871.
16 S. S. Shaik and M.-H. Whangbo, *Inorg. Chem.*, 1986, **25**, 1201.
17 R. E. Peierls, *Quantum Theory of Solids*, Oxford University Press, London, 1955, p. 108.
18 H. W. Ruhle and M. F. Hawthorne, *Inorg. Chem.*, 1968, **7**, 2279.
19 M. F. Hawthorne, D. C. Young, T. D. Andrews, D. V. Howe, R. L. Pilling, A. D. Pitts, M. Reintjes, L. F. Warren, jun. and P. A. Wegner, *J. Am. Chem. Soc.*, 1968, **90**, 879.
20 T. Mallah, C. Hollis, S. Bott, M. Kurmoo, P. Day, M. Allan and R. H. Friend, *J. Chem. Soc., Dalton Trans.*, 1990, 859.
21 D. M. P. Mingos, in *Comprehensive Organometallic Chemistry*, eds. G. Wilkinson, F. G. A. Stone and E. W. Abel, Pergamon, Oxford, 1982, vol. 3, ch. 19, pp. 32, 33.
22 A. J. Gordon and R. A. Ford, *The Chemist's Companion: A Handbook of Practical Data, Techniques and References*, Wiley-Interscience, New York, 1972.
23 D. A. Stephens, A. E. Rehan, S. J. Compton, R. A. Barkhau and J. M. Williams, *Inorg. Synth.*, 1986, **24**, 135.
24 G. M. Sheldrick, SHELXTL PC, Version 4.2, Siemens Analytical X-Ray Instruments Inc., Madison, WI, 1990.

Received 28*th February* 1995; *Paper* 5/01204J